PCCP

ROYAL SOCIETY OF CHEMISTRY

PAPER

View Article Online
View Journal

Cite this: DOI: 10.1039/c9cp04490f

Published on 01 November 2019. Downloaded by University of Warwick on 11/1/2019 11:19:51 AM.

Work function of GaAs(*hkl*) and its modification using PEI: mechanisms and substrate dependence†

Samuel D. Seddon,[a] Christopher Benjamin,[a] James I. Bryant,[a] Christopher W. Burrows,[a] Marc Walker,[a] Graham Matheson,[bc] Jesus Herranz,[b] Lutz Geelhaar[b] and Gavin R. Bell *[a]

Received 13th August 2019,
Accepted 21st October 2019

DOI: 10.1039/c9cp04490f

rsc.li/pccp

Spin-coating of poly(ethylenimine) (PEI) has been used to reduce the work function of GaAs (001), (110), (111)A and (111)B. The magnitude of the reduction immediately after coating varies significantly from 0.51 eV to 0.69 eV and depends on the surface crystal face, on the GaAs bulk doping and on the atomic termination of the GaAs. For all samples, the work function reduction shrinks in ambient air over the first 20 hours after spin coating, but reductions around 0.2–0.3 eV persist after 1 year of storage in air. Core-level photoemission of thin film PEI degradation in air is consistent with a two-stage reaction with CO_2 and H_2O previously proposed in carbon capture studies. The total surface dipole from PEI coating is consistent with a combination of internal neutral amine dipole and an interface dipole whose magnitude depends on the surface termination. The contact potential difference measured by Kelvin probe force microscopy on a cleaved GaAs heterostructure is smaller on p-doped regions. This can be explained by surface doping due to the PEI, which increases the band bending on p-doped GaAs where Fermi level pinning is weak. Both surface doping and surface dipole should be accounted for when considering the effect of PEI coated on a semiconductor surface.

1 Introduction

The work function is a fundamental materials parameter which strongly influences energy level alignment in heterostructures, in particular band offsets at semiconductor heterointerfaces and barrier heights for metal–semiconductor junctions.[1] Such interfaces include those found in organic–inorganic hybrid structures,[2–4] which are of increasing interest in a diverse range of applications.[5–7] Band offset engineering is often critical to optimise charge and exciton transport in such a hybrid device.[8] Hybrid organic–inorganic solar cells are an important example. Using polymers as a surface modifier to control the work function of semiconductors can act to reduce resistances across interfaces,[2,9] as wide gap organic semiconductors with low carrier densities may be associated with strong injection barriers.[10] Improvements in band alignment at interfaces, *e.g.* by work function control,[11] can lead to increased solar power conversion efficiency[12] as recombination rates are reduced[12,13] and injection improves.[14]

[a] Department of Physics, University of Warwick, Coventry, CV4 7AL, UK. E-mail: gavin.bell@warwick.ac.uk; Tel: +44 (0)2476523489
[b] Paul-Drude-Institut für Festkörperelektronik, Leibniz-Institut im Forschungsverbund Berlin e.V., Hausvogteiplatz 5-7, 10117, Berlin, Germany
[c] University of Washington, Seattle, WA, USA

† Electronic supplementary information (ESI) available. See DOI: 10.1039/c9cp04490f

As a method of work function control, Zhou *et al.*[15] first showed in 2012 that ultra-thin films of both poly(ethylenimine) (PEI) and poly(ethylenimine)ethoxylated (PEIE) act to reduce the work functions of various metals and oxides plus graphene and PEDOT:PSS. The values of work function reduction were clustered around 1 eV with a range 0.41 to 1.63 eV reported. This ‘‘universal’’ work function reduction effect was explained through a combination of the intrinsic dipole moment of neutral amine groups in the molecular overlayer and an interface dipole produced through fractional electron donation to the surface.[15–18] Kim *et al.* used a thin (2 nm) PEI interlayer in a hybrid solar cell to reduce the work function of a PEDOT:PSS electrode from 5.1 eV to 3.97 eV.[19] Yan *et al.* incorporated PEI into a hybrid solar cell, reducing the work function of an ITO electrode.[20] In agreement with Zhou *et al.* they found no improvement in work function reduction for thicker PEI films (up to 10 nm) but such films inhibited device performance due to the electrical resistance of the PEI. Both groups achieved strong improvements in device performance due to work function control *via* PEI layers.

The structure of branched PEI can be seen in Fig. 1(i). PEI has been frequently used as an electron injector,[22–24] acting as a surface n-dopant.[25–28] This surface doping effect has been utilized in organic thin film transistors.[29,30] Apart from organic–inorganic

Published on 01 November 2019. Downloaded by University of Warwick on 11/1/2019 11:19:51 AM.

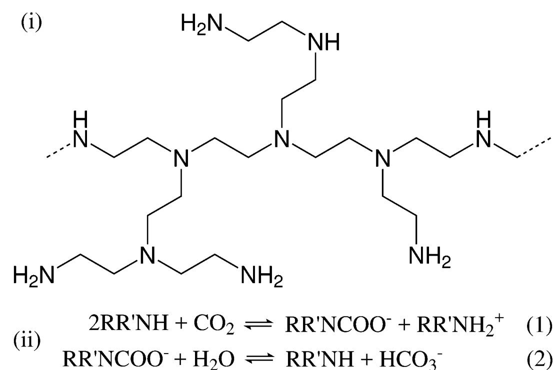

Fig. 1 Structure of branched PEI (i), and the two-stage chemical reaction of PEI with CO_2 (ii), proposed by Yu *et al.*[21]

electronics PEI has been used to control morphology in ZnO films.[31] Before its potential applications in hybrid organic electronics were mooted, PEI was extensively investigated as a carbon capture material.[18,32–41] Suggested reaction mechanisms between CO_2 and PEI are shown in Fig. 1(ii).[21,32] A two stage reaction was suggested: products from the first stage (CO_2) react with water, returning some of the initial reactant (R/R′ refer to carbon chains). Degradation in ambient air of PEI films used as dopants for multilayer MoS_2 films has been reported by Du *et al.*,[28] with a timescale on the order of six hours and no net doping remaining after four days. Conversely, Zhou *et al.* reported less than 0.2 eV drop in work function reduction for PEIE on ITO over 4 weeks in ambient air.

GaAs is an important technological semiconductor material employed primarily in optoelectronics. GaAs has also been used in hybrid organic–inorganic devices such as solar cells,[42,43] plasmonic structures[44] and polariton lasers.[45] The work function of oxide-free GaAs(*hkl*) has been studied by photoemission in ultra-high vacuum (UHV).[46,47] In UHV conditions, GaAs is frequently used as a negative electron affinity photocathode for spin-polarised electron beam generation, by the application of a strong surface dipole through Cs and O adsorption. In ambient conditions, the GaAs work function has been altered by treatment with benzoic acid derivatives.[16]

In this work we explore PEI ultra-thin films spin-coated on to GaAs(*hkl*) surfaces as a work function modifier. We find that PEI indeed reduces the GaAs work function significantly but that the magnitudes are different on different crystal faces, and different for native oxide-coated GaAs(001) compared with etched GaAs(001). These observations support the idea that the total surface dipole due to PEI adsorption includes a contribution from an interface dipole (charge transfer between surface and PEI) as well as any dipole moment internal to the PEI film. Furthermore, the work function reductions changed for differently doped regions of a GaAs heterostructure cleaved to reveal a (110) surface. This can be related to the surface doping effect of PEI adsorption. We also study the decay of work function reduction over time in ambient air, using X-ray photoelectron spectroscopy (XPS) to characterise the changing surface chemistry.

2 Results and discussion

2.1 Concentration dependence

Fig. 2 shows the work function reduction due to spin-coating PEI from solutions of varying concentration. Aqueous solutions were mixed in concentrations ranging from 0.1% to 3.2%. Solutions were immediately spin-coated onto freshly prepared GaAs(110) to be measured by Kelvin probe. For concentrations up to 0.8% the work function decreases linearly (red line) before plateauing at around 0.67 eV for values up to 3.2% (green line). This behaviour is consistent with an increasing surface coverage of PEI with higher concentration solution. This leads to a proportional increase in work function reduction averaged over the Kelvin probe's 2 mm diameter tip. Once the substrate is fully covered with the optimum thickness, further adsorption of PEI does not continue to decrease the work function. Our results agree with previous work. Yan *et al.* increased PEI film thickness on ITO and found a linear decrease in work function followed by a plateau above 2 nm thickness.[20] Zhou *et al.* observed PEIE islands on ITO on top of a thin continuous layer; by gentle washing, these islands could be removed without affecting the work function reduction by more than 0.1 eV. Huang *et al.*[23] found an optimal work function reduction for PEI on indium oxide using concentrations between 1% and 1.5%, in good agreement with our data. All of these results suggest that only PEI molecules in close proximity to the substrate surface contribute to the work function reduction. In the rest of our paper we report results for fixed PEI concentration of 0.8%, which maximises work function reduction while minimising any complications due to multi-layer stacking of PEI molecules. Note that the 0% concentration point in Fig. 2 (defined zero change of work function) corresponds to untreated GaAs (Table 1), not to a sample which has been subjected to spin-coating with pure water.

2.2 Crystal face and time dependence

The work functions of four low-index orientations of untreated GaAs are presented in Table 1. Even in the presence of the

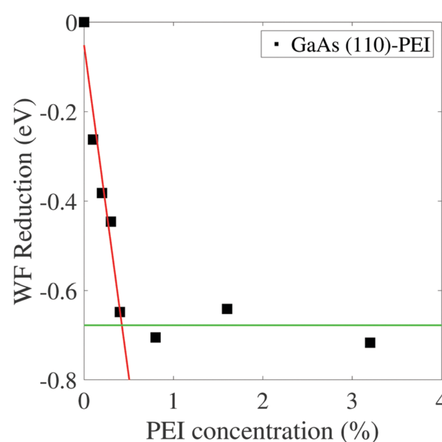

Fig. 2 GaAs(110) work function reduction as a function of PEI concentration. Data points have been plotted with two indicative lines: red indicates increasing work function reduction at concentrations up to 0.8%, green indicates saturated work function reduction for higher concentrations.

Table 1 Tabulated work function values for native oxide-covered n-type low-index GaAs surfaces. Right side columns show work function reductions for three different times after PEI deposition. The central column shows the calculated number of dipoles per GaAs(100) unit mesh due to a fresh PEI coating, as discussed later

Orientation	Native oxide (eV)	Dipoles per unit mesh due to PEI	Work function change due to PEI (eV)		
			Fresh	20 hours	1 year
GaAs(100)	4.06	1.4	−0.63	−0.34	−0.19
GaAs(111)A	4.20	1.2	−0.55	−0.40	—
GaAs(111)B	4.17	1.5	−0.69	−0.51	—
GaAs(110)	4.18	1.6	−0.71	−0.42	−0.27

native oxide there is significant variation of 0.14 eV in the GaAs work function, with GaAs(100) showing significantly lower work function than the other faces. The work function reduction due to PEI coating is also shown in Table 1, immediately after coating, after measuring for 20 hours and after storing for 1 year (data available for two orientations only). Both measurement and storage were in ambient air. The initial work function reduction varies over a range of 0.16 eV. In all cases the work function reduction declines with exposure time to ambient air, *i.e.* the absolute work function moves back towards the native oxide-only value. However, a significant reduction remains even after 1 year exposure to ambient air. The time dependence of work function reduction during the first 20 hours is plotted in Fig. 3. For all crystal faces of GaAs the work function reduction decreases markedly over this period with a declining rate of change. The most rapid loss of work function reduction occurs for GaAs(100), while the (110) surface shows a similar magnitude of decline which occurs more steadily (Fig. 3, red and purple lines). Despite the untreated work function values for GaAs(111)A and GaAs(111)B being nearly identical, upon the application of PEI the work function reduction differs by 0.14 eV. Over the first 20 hours after coating, both the A and B faces degrade at the same rate, roughly maintaining the 0.14 eV split (Fig. 3, blue and green lines).

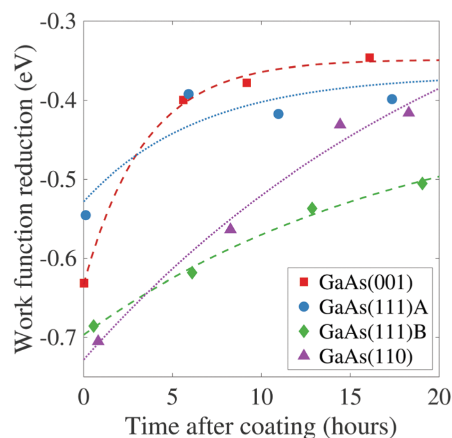

Fig. 3 Work function reduction dependence on air exposure time for PEI coating on low-index GaAs(*hkl*). Lines are guides to the eye.

2.3 Bulk doping dependence

In order to isolate any effect of doping levels on work function reduction due to PEI coating, samples cleaved from a GaAs heterostructure were studied. The heterostructure incorporates p-type (Be-doped) and n-type (Si-doped) layers and was grown in the (001) direction. PEI was spin-coated on to freshly cleaved (110) surfaces which expose the vertical layer sequence. The position-dependent contact potential difference[48] (CPD) was then measured by Kelvin probe force microscopy (KPFM). The layer pattern of the heterostructure can be identified unambiguously for different samples since the local CPD depends on the local doping level. By subtracting the local CPD of a PEI coated sample from the corresponding local CPD of a pristine sample, the work function reduction for GaAs(110) can be obtained for the differently doped regions. The position-dependent work function reduction is shown schematically for six regions of the heterostructure in Fig. 4 (the full structure is shown in the ESI,†). Note that the KPFM samples were sent from Warwick to Berlin by courier for measurement, which is likely to induce significant degradation; nonetheless, a significant work function reduction is retained.

There is a clear difference between p-type regions, for which the work function is reduced by approximately 0.17 ± 0.01 eV, and the other regions with work function reductions of around 0.27 ± 0.03 eV. The latter values are consistent with those reported in Table 1 for n-type GaAs(110) after one year's storage in air. If the PEI provides a pure surface dipole, only reducing the local vacuum level, one would not expect a change of CPD reduction between differently doped regions. It is clear that the CPD reduction on p-type regions is around 0.1 eV smaller than on other regions: this apparent discrepancy is discussed in Section 2.7.

2.4 Surface termination dependence

In order to further explore electronic interaction between the PEI overlayer and substrate surface condition, the native oxide of GaAs(100) was etched using hydrochloric acid.[49] Table 2 shows an XPS elemental quantification of oxidised and etched samples (total intensity normalised by atomic sensitivity factor). The Ga-rich native oxide of GaAs(100) is replaced with a principally Cl-terminated surface. A higher binding energy component

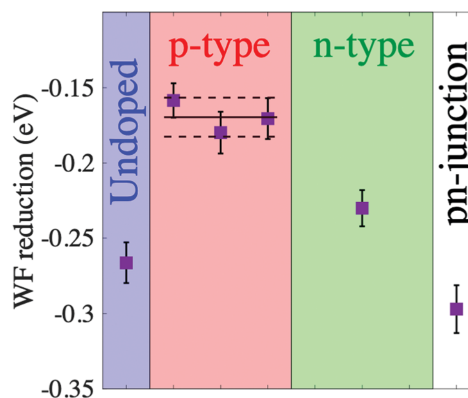

Fig. 4 Position-dependent work function reduction due to PEI coating on the (110) cleaved surface of a GaAs heterostructure.

Published on 01 November 2019. Downloaded by University of Warwick on 11/1/2019 11:19:51 AM.

Published on 01 November 2019. Downloaded by University of Warwick on 11/1/2019 11:19:51 AM.

Table 2 Relative region intensities ratios for GaAs(100) with native oxide and after etching with HCl

Region	Pre-etch (%)	Post-etch (%)
C 1s	21.2	9.6
O 1s	31.5	5.2
Ga 3d	26.4	38.6
As 3d	20.9	37.2
Cl 2p	0.0	9.4

appears in the Ga 3d spectra after etching, indicating that Cl is bonded to Ga at the surface (see ESI†). Residual O and C signals are due to the rinsing/drying and transfer to the XPS system after acid etching. The absolute work function measured by Kelvin probe increases by 0.33 eV after etching. After 0.8% PEI solution was spin-coated on to etched GaAs(001), the work function reduction was 1.02 eV, compared to 0.63 eV coated directly onto the native oxide (Table 1). The absolute values of the work function after PEI coating are very similar comparing the etched sample and the native oxide, within 0.06 eV of each other. This suggests that the interaction between the PEI overlayer and substrate has been changed by converting the native oxide surface termination to a (Ga,Cl) surface, which has increased the total surface dipole induced by the PEI. Note that our XPS data show no change of Cl surface concentration between etched-rinsed and etched-rinsed-spin-coated samples, so that the reported work function changes, as well as absolute value comparisons are self-consistent.

2.5 Degradation

Native oxide-covered GaAs(110) samples were coated in PEI and studied by XPS within seven days after coating and also after storage in air for two months and ten months. Long-term degradation data were not available for other orientations, but as the mechanism involves the internal chemistry of the (non-epitaxial) PEI film we believe it will not differ greatly on different GaAs faces. The C 1s, O 1s, N 1s, Ga 2p, Ga 3d and As 2p regions were acquired. The normalised intensities of the key surface elements, *i.e.* C : N and O : N 1s ratios, changed over time. For the freshest PEI sample, the C : N ratio was approximately 3 : 1, and this increased steadily with storage time, rising to 4 : 1 (2 months) then 5 : 1 (10 months). The O : N ratio rose more sharply, from around 1 : 3 (fresh) to 1 : 1 (2 months) and 3 : 2 (10 months). There is no evidence for loss of nitrogen from the surface and so the increases in O and C are ascribed to adsorption from the ambient air along with chemical reactions within the PEI film. Further insight into these processes can be gained from examining the chemically shifted components of the C and N 1s XPS peaks.

In Fig. 5 the three C 1s and N 1s spectra are shown with fitted components identified by colour in the legend. In the C 1s, components assigned to C–O and C═O bonding are present throughout although oxygen is not a constituent of the PEI molecule. These components are due to atmospheric contamination, initially from the spin coating and Kelvin probe experiments performed in air, and later from subsequent storage in ambient conditions. The dominant component in the C 1s region of the freshly deposited sample [Fig. 5(a)] at binding energy 287.0 eV is attributed to C–N, which does not commonly appear due to atmospheric contamination. This clearly shows the presence of PEI on the surface, in which all C atoms are C–N bonded. Similarly in the N 1s [Fig. 5(d)], the primary component at 400.3 eV is attributed to

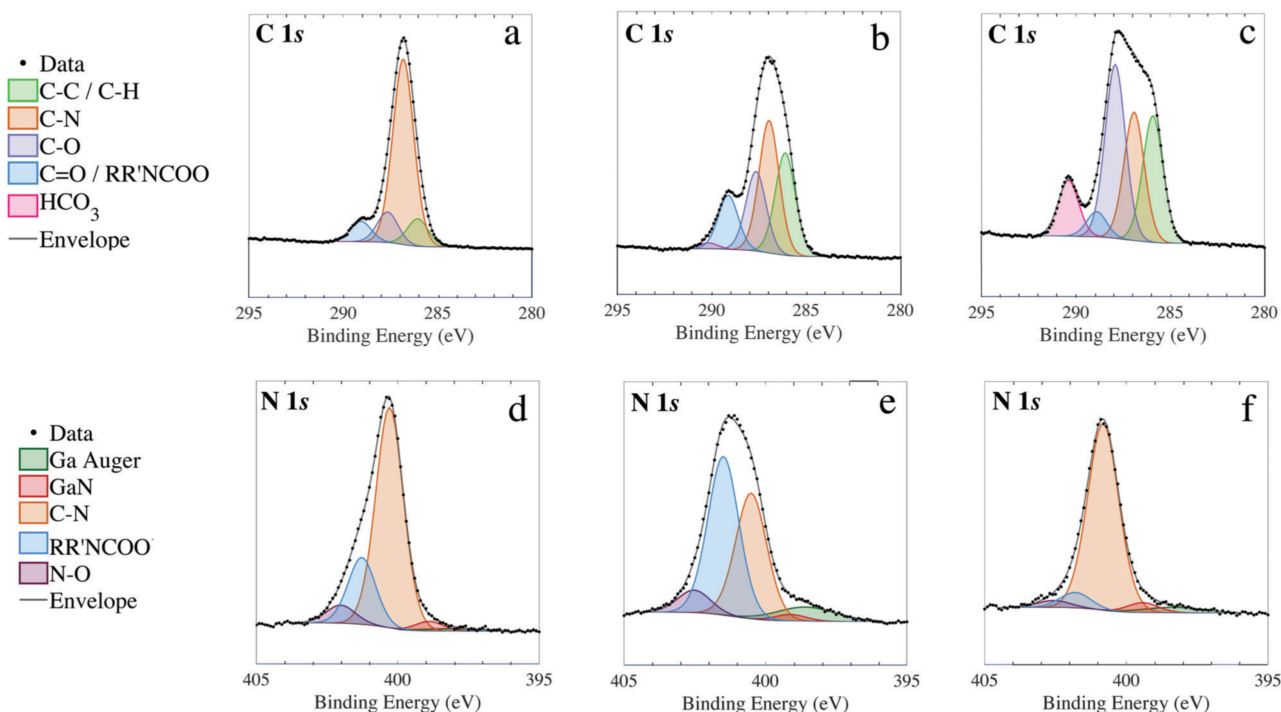

Fig. 5 C 1s and N 1s XPS spectra of a PEI layer deposited on GaAs(110) with native oxide surface after different storage times in air: 1 week (a and d), 2 months (b and e) and 10 months (c and f). Chemically shifted components are identified by colour.

 This journal is © the Owner Societies 2019

Published on 01 November 2019. Downloaded by University of Warwick on 11/1/2019 11:19:51 AM.

the C–N environment. At 7 days, the C–N component forms 70% of the total C 1s intensity, while at 2 months this contribution has dropped to 36%. A further reduction to 25% was observed after 10 months' storage. The reduction of the C–N fraction occurs alongside an increase of intensity at higher and lower binding energies in the C 1s envelope [Fig. 5(b)]. This suggests a surface chemical reaction which changes C–N to other C species over time, principally C–H/C–C, C–O and C=O. The corresponding N 1s spectrum [Fig. 5(e)] also shows a strong reduction in pure C–N bonding, while an increase in a component at 401.5 eV is observed. This component is subsequently reduced in intensity after 10 months storage leading to a simpler peak shape dominated by a slightly broadened C–N component. At 10 months, the C 1s envelope retains a complex array of components with a strong peak attributed to HCO_3 at binding energy 290.2 eV.

The two-stage CO_2 reaction mechanism shown in Fig. 1 gives a plausible basis for these XPS observations. In particular, the intermediate state after CO_2 reaction (1) contains a N–(C=O)–O group and this component of the C 1s envelope is indeed observed to increase at 289.1 eV, increasing from 7.8% to 14.5% during storage over 2 months [Fig. 5(b), blue peak]. This component overlaps with the C=O component originally present due to contamination. Water vapour from the ambient air can induce reaction (2) producing HCO_3, as observed over the longer storage period [Fig. 5(c), pink peak]. The N–(C=O)–O intermediate intensity decreases again, back to its initial level due to the C=O contamination. This two stage degradation process is also consistent with the N 1s spectra. The significant increase of the component at 401.5 eV from 21% to 46% Fig. 5(d to e) is ascribed to the CO_2 reaction (1) product with altered nitrogen environments, as seen in the reaction mechanism in Fig. 1. However, the H_2O reaction (2) returns nitrogen to original PEI-like chemical environments, hence the reduction again of the 401.5 eV component after 10 months Fig. 5(f). The persistence of C–N components in both C 1s and N 1s is in agreement with the persistent work function reduction even after 1 year of storage.

2.6 Surface dipole

Different surface reconstructions of GaAs(100) in UHV change its ionization energy by up to 0.5 eV, with more As-rich surfaces showing higher values.[50] This is due to the surface dipole induced by the polar Ga–As bond. For the same reason, clean GaAs(111)A and (111)B surfaces in UHV show work function[46] or electron affinity[47] differing by several tenths of an eV. However, after ion sputtering of GaAs(111), the surface potentials no longer depend on the crystal face.[46,47] Ion sputtering causes the near-surface region to become completely amorphous, and this observation is consistent with a loss of net surface dipole in the non-crystalline region, independent of the underlying bulk crystal structure. The behaviour of the (111)A, (111)B and (110) oxidised surfaces measured here is similar, with the amorphous native oxide layer suppressing any differences in the surface dipole from bond polarity effects. Indeed, the absolute values of the ambient work functions are only around 0.13 eV smaller than the common amorphous-surface UHV work function (4.31 ± 0.05 eV). This consistent difference is presumably due to the presence of more electronegative oxygen within the amorphous surface layer. However, the native oxide of GaAs(100) is apparently somewhat different in nature, with a work function around 0.12 eV lower than the other faces (Table 1). This is possibly due to bond orientation or an excess of less electronegative Ga in the oxide (Table 2) which results in a stronger net surface dipole and lower work function.

The Helmholtz equation can be used to estimate the density N of PEI-induced dipoles.[16,51]

$$N = \frac{\Delta V \varepsilon_0 \varepsilon_r}{\mu \cos \theta} \quad (1)$$

In eqn (1), ΔV is the change in work function, ε_r and ε_0 are the relative and free space permittivities respectively, θ is the dipole direction relative to the surface normal and μ is the magnitude of the dipole. Then N is the number of dipoles per unit area. We have taken ε_r to be 9 (based on experiment[52]), μ as 1.72 D (assuming a C–N bond in neutral amine group[53]), and θ as zero. Across the surfaces studied, N lies in the range $8.7 \pm 1.1 \times 10^{18}$ m^{-2}, which we normalise to the GaAs(100) unit mesh size and show in Table 1. The different crystallographic primitive unit mesh sizes on the (111), (110) and (100) faces are not relevant given the presence of the amorphous native oxide, and GaAs(100) is chosen as a convenient normalisation. The density lies in the range 1.2 to 1.6 neutral amine dipoles per unit mesh. This is consistent with a densely packed monolayer of PEI with a reasonably well defined adsorption geometry, having N–C bonds oriented out of the surface plane, as proposed by Zhou *et al.*[15] The variation across the different crystal faces is interesting and can be ascribed to a varying contribution of an interface dipole due to charge transfer between the adsorbed PEI and the substrate atoms. These contributions were calculated by Zhou *et al.*[15] for idealised interfaces, and were found to be similar in magnitude for adsorption on Au and different ZnO surfaces. In the present case, the variation is rather smaller than the absolute values, *i.e.* the range is 1.4 ± 0.2 dipoles per mesh. This can again be ascribed to the presence of the amorphous oxide which largely masks the polar bulk structure. Nonetheless some variation remains, which may be due to different levels of electron transfer to terminating O atoms from within the bulk GaAs. Similarly, the effective dipole strength is around 10% larger after HCl etch on GaAs(100). Replacing the Ga-rich native oxide with Ga–Cl termination leads to increased electron transfer from N to the surface atoms which adds to the interface dipole.

2.7 Surface doping

For a semiconductor, the local vacuum level relative to the band edges, and hence measured CPD, depends on the location of the Fermi level within the band gap, which varies with bulk doping and temperature. Surface band bending also affects the CPD, and for many materials the surface Fermi level is "pinned", or at least restricted to a narrow range of mid-gap energies. For heavily n-doped GaAs,[54] the density of ionised surface acceptor states is around 10^{13} cm^{-2} and the surface Fermi level lies between 0.5 eV above the valence band maximum and mid-gap.

Published on 01 November 2019. Downloaded by University of Warwick on 11/1/2019 11:19:51 AM.

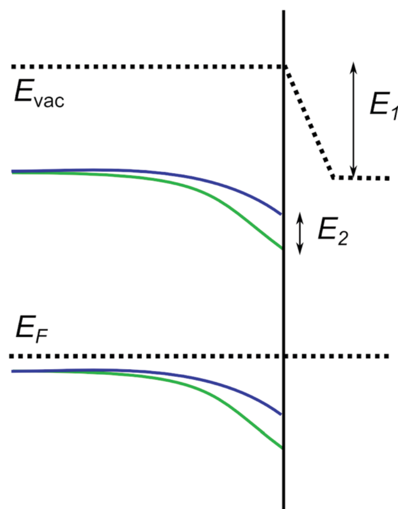

Fig. 6 Schematic energy level alignment for p-type GaAs with PEI acting both as a surface dipole and surface donor. The horizontal direction is depth, with the vertical line representing the sample surface. Dotted lines show the Fermi and vacuum levels. Curves represent the bent band edges for native oxide (blue) and oxide plus surface donor (green).

Conversely, on strongly p-doped GaAs far fewer surface states are ionised and the surface charge density is two orders of magnitude smaller, insufficient to firmly pin the surface Fermi level.[55] A extra surface donor adds to the density of pre-existing ionised donor-like surface states and, except in the limit of strong pinning, changes the surface Fermi level. This is illustrated schematically in Fig. 6. Weak downward band bending at the surface (blue curves) is increased by the addition of a PEI surface donor (green curves) leading to a increase of ionization potential and electron affinity by amount E_2. This acts against the work function reduction E_1 induced by the PEI surface dipole, lowering the measured CPD reduction due to PEI. However, strong Fermi level pinning on n-type GaAs means that there is a negligible change in the neutralisation of acceptor-like surface states so that the CPD change measured is just E_1. This is consistent with our experimental observations in Fig. 4 where the work function reduction is smaller on p-type regions of the heterostructure by around 0.1 eV. More detailed calculations of the electrostatics, *e.g.* using finite element methods to account for screening and probe size in KPFM, would be required to quantify this effect. However the present results highlight the need to account for both surface doping and surface dipole from PEI when considering the overall effect on CPD for a semiconductor with weak surface Fermi level pinning.

3 Conclusions

Spin-coated PEI monolayers have been used to modify the work function of GaAs. Work function reductions on the range 0.55 to 0.71 eV have been found dependent on the crystal face of the GaAs. The strength of the surface dipole is consistent with the presence of around 1.4 neutral amine dipoles per GaAs unit mesh, plus a weaker interface dipole which varies with crystal face and surface termination. The work function reduction degrades over time when samples are stored in air. Chemical shifts of N 1s and C 1s measured in XPS for air-stored samples are consistent with previously proposed reaction pathways between PEI and CO_2 and H_2O. Work function reduction persists even after storage in air for 1 year. A smaller work function reduction on p-type regions of a cleaved heterostructure can be explained by the surface doping effect of PEI causing additional band bending, which reduces the measured CPD. In general, both the surface doping and surface dipole effects should be considered when semiconductor materials (both organic and inorganic) are treated with electronically active asdorbates such as PEI.

4 Experimental details

The samples used were cleaved from epi-ready wafers, and the samples used for repeat measurements were all cleaved from the same wafer. All the GaAs samples were n-type, silicon doped. The bulk carrier densities were measured at room temperature using the Hall effect in van der Pauw geometry, and these lay in the range $(1.4\text{–}5.4) \times 10^{18}$ cm^{-3}. The change of bulk Fermi level position over this carrier density range is less than 20 meV (see ESI†) and so work function differences measured here are due to surface effects. Samples were rinsed in a 1 : 1 acetone and isopropanol mix before blow drying with dry nitrogen. To remove GaAs native oxide, samples were submerged in a 2 : 1 H_2O : HCl solution for 30 seconds before being thoroughly rinsed in deionised water. They were then immediately measured in the Kelvin probe or spin-coated with PEI. For PEI coating, 0.1% to 3.2% PEI into water (weight per volume) branched PEI solutions were produced, with most samples treated using a 0.8% solution. PEI was deposited using a spin coater from Ossila Ltd, UK. Samples were spun up to 1000 rpm, then the PEI was deposited at the start of a 60 s cycle at 5000 rpm, followed by an 800 rpm cycle for 10 s. Samples were not annealed after PEI coating. The GaAs heterostructure included Be-doped and Si-doped layers with doping levels around 10^{17} cm^{-3}, 10^{18} cm^{-3} and 10^{19} cm^{-3}, and with thicknesses 200 nm to 250 nm. Additional AlAs spacer layers were present: see ESI,† for the full structure.

Work function measurements were performed in ambient air using a commercial Kelvin probe system fitted with a 2 mm gold tip. KPFM measurements were performed in nitrogen atmosphere using a 20 nm tip diameter Pt-Ir probe. XPS measurements were performed using a Kratos Axis Ultra DLD spectrometer with monochromated Al k_α X-rays. Further details of all three methods, such as XPS fitting procedures and Kelvin probe tip work function calibration/uncertainty quantification, are given in the ESI.†

Conflicts of interest

There are no conflicts to declare.

Acknowledgements

J. I. B. was supported by the Doctoral Training Partnership (EPSRC, UK). G. M. is grateful for a scholarship funded by

This journal is © the Owner Societies 2019

Deutscher Akademischer Austauschdienst in the program Research Internships in Science and Engineering and thanks M. Heilmann for KPFM training.

Published on 01 November 2019. Downloaded by University of Warwick on 11/1/2019 11:19:51 AM.

References

1 A. Khan, *Mater. Horiz.*, 2016, **3**, 7.
2 G. Yu, J. Gao, J. C. Hummelen, F. Wudl and A. J. Heeger, *Science*, 1995, **270**, 1789–1791.
3 C. H. Chen and I. Shih, *J. Mater. Sci.: Mater. Electron.*, 2006, **17**, 1047–1053.
4 M. H. Futscher, T. Schultz, J. Frisch, M. Ralaiarisoa, E. Metwalli, M. V. Nardi, P. Müller-Buschbaum and N. Koch, *J. Phys.: Condens. Matter*, 2019, **31**, 064002.
5 N. Guijarro, M. S. Prévot and K. Sivula, *Phys. Chem. Chem. Phys.*, 2015, **17**, 15655–15674.
6 S. H. Mir, L. A. Nagahara, T. Thundat, P. Mokarian-Tabari, H. Furukawa and A. Khosla, *J. Electrochem. Soc.*, 2018, **165**, B3137–B3156.
7 R. Naaman, *Phys. Chem. Chem. Phys.*, 2011, **13**, 13153–13161.
8 S. Blumstengel, H. Glowatzki, S. Sadofev, N. Koch, S. Kowarik, J. P. Rabe and F. Henneberger, *Phys. Chem. Chem. Phys.*, 2010, **12**, 11642–11646.
9 C. G. Tang, M. C. Y. Ang, K.-K. Choo, V. Keerthi, J.-K. Tan, M. N. Syafiqah, T. Kugler, J. H. Burroughes, R.-Q. Png, L.-L. Chua and P. K. H. Ho, *Nature*, 2016, **539**, 536–540.
10 E. D. Gomez and Y.-L. Loo, *J. Mater. Chem.*, 2010, **20**, 6604–6611.
11 R. Cao, *J. Vac. Sci. Technol., B: Microelectron. Nanometer Struct.--Process., Meas., Phenom.*, 1987, **5**, 998.
12 G. Li, V. Shrotriya, J. Huang, Y. Yao, T. Moriarty, K. Emery and Y. Yang, *Nat. Mater.*, 2005, **4**, 864–868.
13 R. King, R. Sinton and R. Swanson, *IEEE Trans. Electron Devices*, 1990, **37**, 365–371.
14 C. V. Hoven, R. Yang, A. Garcia, V. Crockett, A. J. Heeger, G. C. Bazan and T.-Q. Nguyen, *Proc. Natl. Acad. Sci. U. S. A.*, 2008, **105**, 12730–12735.
15 Y. Zhou, C. Fuentes-hernandez, J. Shim, J. Meyer, A. J. Giordano, H. Li, P. Winget, T. Papadopoulos, H. Cheun, J. Kim, M. Fenoll, A. Dindar, W. Haske, E. Najafabadi, T. M. Khan, H. Sojoudi, S. Barlow, S. Graham, J.-l. Brédas, S. R. Marder, A. Kahn and B. Kippelen, *Science*, 2012, **873**, 327–332.
16 S. Bastide, R. Butruille, D. Cahen, A. Dutta, J. Libman, A. Shanzer, L. Sun and A. Vilan, *J. Phys. Chem.*, 1997, **5647**, 2678–2684.
17 S. Stolz, M. Scherer, E. Mankel, R. Lovrinčić, J. Schinke, W. Kowalsky, W. Jaegermann, U. Lemmer, N. Mechau and G. Hernandez-Sosa, *ACS Appl. Mater. Interfaces*, 2014, **6**, 6616–6622.
18 H. Zhang, A. Goeppert, G. K. S. Prakash and G. Olah, *RSC Adv.*, 2015, **5**, 52550–52562.
19 K. M. Kim, S. Ahn, W. Jang, S. Park, O. O. Park and D. H. Wang, *Sol. Energy Mater. Sol. Cells*, 2018, **176**, 435–440.
20 L. Yan, Y. Song, Y. Zhou, B. Song and Y. Li, *Org. Electron.*, 2015, **17**, 94–101.
21 C. H. Yu, C. H. Huang and C. S. Tan, *Aerosol Air Qual. Res.*, 2012, **12**, 745–769.
22 T. Davidson-Hall and H. Aziz, *Nanoscale*, 2018, 2623–2631.
23 W. Huang, L. Zeng, X. Yu, P. Guo, B. Wang, Q. Ma, R. P. Chang, J. Yu, M. J. Bedzyk, T. J. Marks and A. Facchetti, *Adv. Funct. Mater.*, 2016, **26**, 6179–6187.
24 Y. H. Kim, T. H. Han, H. Cho, S. Y. Min, C. L. Lee and T. W. Lee, *Adv. Funct. Mater.*, 2014, **24**, 3808–3814.
25 M. Shim, A. Javey, N. W. Shi Kam and H. Dai, *J. Am. Chem. Soc.*, 2001, **123**, 11512–11513.
26 C. Klinke, J. Chen, A. Afzali and P. Avouris, *Nano Lett.*, 2005, **5**, 555–558.
27 P. Li, L. Cai, G. Wang, D. C. Zhou, J. Xiang, Y. J. Zhang, B. F. Ding, K. Alameh and Q. L. Song, *Synth. Met.*, 2015, **203**, 243–248.
28 Y. Du, H. Liu, A. T. Neal, M. Si and P. D. Ye, *IEEE Electron Device Lett.*, 2013, **34**, 1328–1330.
29 B. Sun, W. Hong, E. Thibau, H. Aziz, Z. H. Lu and Y. Li, *Org. Electron.*, 2014, **15**, 3787–3794.
30 C. R. Newman, C. D. Frisbie, D. A. D. S. Filho, J. L. Brédas, P. C. Ewbank and K. R. Mann, *Chem. Mater.*, 2004, **16**, 4436–4451.
31 X. Hu, Y. Masuda, T. Ohji and K. Kato, *Appl. Surf. Sci.*, 2009, **255**, 6823–6826.
32 S. Satyapal, T. Filburn, J. Trela and J. Strange, *Energy Fuels*, 2001, **15**, 250–255.
33 A. Goeppert, M. Czaun, R. B. May, G. K. Prakash, G. A. Olah and S. R. Narayanan, *J. Am. Chem. Soc.*, 2011, **133**, 20164–20167.
34 A. Goeppert, M. Czaun, G. K. Surya Prakash and G. A. Olah, *Energy Environ. Sci.*, 2012, **5**, 7833–7853.
35 W. Chaikittisilp, R. Khunsupat, T. T. Chen and C. W. Jones, *Ind. Eng. Chem. Res.*, 2011, **50**, 14203–14210.
36 S. Choi, M. L. Gray and C. W. Jones, *ChemSusChem*, 2011, **4**, 628–635.
37 X. Yan, L. Zhang, Y. Zhang, K. Qiao, Z. Yan and S. Komarneni, *Chem. Eng. J.*, 2011, **168**, 918–924.
38 T. Zhu, S. Yang, D. K. Choi and K. H. Row, *Korean J. Chem. Eng.*, 2010, **27**, 1910–1915.
39 Q. Chen, F. Fan, D. Long, X. Liu, X. Liang and W. Qiao, *Ind. Eng. Chem. Res.*, 2010, **49**, 11408–11414.
40 W. J. Son, J. S. Choi and W. S. Ahn, *Microporous Mesoporous Mater.*, 2008, **113**, 31–40.
41 X. Xu, C. Song, J. M. Andresen, B. G. Miller and A. W. Scaroni, *Energy Fuels*, 2002, **16**, 1463–1469.
42 X. Fan, M. Zhang, X. Wang, F. Yang and X. Meng, *J. Mater. Chem. A*, 2013, **1**, 8694–8709.
43 K. Cheng, H. Pan, S. Yu, W. Weng, Y. Lai, Y. Lin, Y. Chen, M. Li, H. W. Hu, P. Yu and H. Meng, *IEEE 40th Photovoltaic Specialist Conference (PVSC)*, 2014, pp. 1519–1521.
44 M. Kaveh, Q. Gao, C. Jagadish, J. Ge, G. Duscher and H. P. Wagner, *Nanotechnology*, 2016, **27**, 485204.
45 G. G. Paschos, N. Somaschi, S. I. Tsintzos, D. Coles, J. L. Bricks, Z. Hatzopoulos, D. G. Lidzey, P. G. Lagoudakis and P. G. Savvidis, *Sci. Rep.*, 2017, **7**, 11377.
46 J. M. Chen, *Surf. Sci.*, 1971, **25**, 305–314.
47 W. Ranke, *Phys. Rev. B: Condens. Matter Mater. Phys.*, 1983, **27**, R7807.

Published on 01 November 2019. Downloaded by University of Warwick on 11/1/2019 11:19:51 AM.

48 L. Polak and R. J. Wijngaarden, *Phys. Rev. B*, 2016, **93**, 195320.
49 O. E. Tereshchenko, S. I. Chikichev and A. S. Terekhov, *J. Vac. Sci. Technol., A*, 1999, **17**, 2655–2662.
50 K. Hirose, E. Foxman, T. Noguchi and M. Uda, *Phys. Rev. B: Condens. Matter Mater. Phys.*, 1990, **41**, 6076.
51 O. N. Oliveira, D. M. Taylor and H. Morgan, *Thin Solid Films*, 1992, **210–211**, 76–78.
52 I. B. Pehlivan, R. Marsal, P. Georén, C. G. Granqvist and G. A. Niklasson, *J. Appl. Phys.*, 2010, **108**, 1–6.
53 A. C. McClellan, *Tables of Experimental Dipole Moments*, Freeman, San Fransico, 1963.
54 G. S. Chang, W. C. Hwang, Y. C. Wang, Z. P. Yang and J. S. Hwang, *J. Appl. Phys.*, 1999, **86**, 1765–1767.
55 D. Yan, E. Look, X. Yin, F. H. Pollak and J. M. Woodall, *Appl. Phys. Lett.*, 1994, **65**, 186–188.

 This journal is © the Owner Societies 2019